Mesoporous Materials

DOI: 10.1002/ange.201102007

Mesoporous Ferrihydrite-Based Iron Oxide Nanoparticles as Highly Promising Materials for Ozone Removal**

Thomas Mathew, Kenichirou Suzuki,* Yasuhiro Ikuta, Yasutaka Nagai, Naoko Takahashi, and Hirofumi Shinjoh*

Gaseous ozone (O_3) in the troposphere is considered to be one of the most harmful air pollutants in view of its high reactivity and immediate action to the surroundings, which causes both short- and long-term adverse health effect and also disrupts plant growth.[1–3] Materials explored for eliminating O_3 in several applications include activated carbon or carbon-promoted oxide materials, noble-metal-supported catalysts, and various transition-metal oxides.[3–6] These materials have diverse drawbacks: they must often be deposited on high-surface-area metal oxides or mixed with organic additives to enhance their performance, they use expensive metal components, they are not very environmentally friendly, and they are not flexible enough to use as a common choice in a wide range of sectors. Herein, we report for the first time that the two-line ferrihydrite (2LFh) with accessible mesopores can be used as a potential candidate for O_3 removal. The following aspects prompted us to consider mesoporous 2LFh (M2LFh) a judicial choice for O_3 removal: 1) it possesses high surface area and, being in the ferrihydrite (Fh) phase, a much higher percentage of iron sites are at or near the surface than in the bulk;[7–9] 2) with accessible mesopores, Fh nanoparticles have the potential for high adsorption owing to an increased rate of mass transfer to the reactive iron sites, such as we recently reported for their high efficiency in rapidly removing organic contaminants in the air;[10] and 3) as an oxyhydroxide of iron, Fh is environmentally friendly and can be applied in various sectors. We also show herein that the presence of Fh nanoparticles in disordered mesostructured iron oxide has a significant effect on the bulk and surface structure of the material and on the activity. Our findings can contribute toward designing Fh-based materials as new potential catalysts for rapid removal of O_3 and its decomposition.

M2LFh was prepared according to a reported procedure[10] by assembly of Fh nanoparticles in 1-propanol in the presence of polyoxyethylene (20) cetyl ether template. Additionally, a mesostructured semicrystalline iron oxide composed of amorphous Fh nanoparticles and crystalline γ-Fe_2O_3 phase (MSIO) and a crystalline iron oxide with no well-defined mesopores (CIO) were prepared for comparison. MSIO was prepared through a sol–gel process in which iron nitrate, oleic acid, a triblock polymer template (F127), and 1-propanol were mixed, with subsequent ageing and calcination. CIO was prepared by assembly of iron oxyhydroxide in a water/ethylene glycol mixture in the presence of cetyltrimethylammonium bromide. Details of MSIO and CIO synthesis are given in the Supporting Information.

The wide-angle XRD pattern of M2LFh (Figure 1 a,A) shows two broad reflections of the 2LFh phase. Although the amorphous Fh-phase reflections in the XRD pattern of MSIO (Figure 1 a,B) were disguised to a great extent by the crystalline peaks of γ-Fe_2O_3, the analysis of the Mössbauer spectrum (see Table S1 in the Supporting Information) indicated that MSIO is composed of about 47% Fh and 53% γ-Fe_2O_3. In the case of CIO, all the diffraction peaks (Figure 1 a,C) are in good agreement with the standard XRD pattern of the hexagonal phase of α-Fe_2O_3 (JCPDS No. 80-2377), and the Mössbauer result (see Table S1 in the Supporting Information) gives further confirmation of this characteristic phase. A broad, low-angle XRD peak at $2\theta = 0.5$–$3.0°$ (Figure S1 in the Supporting Information) and a characteristic type IV isotherm with a homogeneous pore size distribution in the range 4–6 nm by N_2 adsorption analyses (Figure S2 in the Supporting Information) are critical pieces

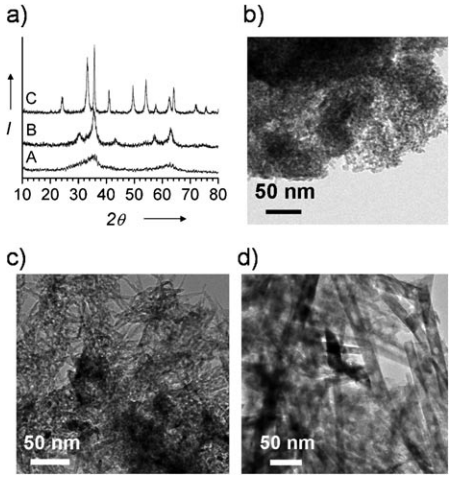

Figure 1. a) Wide-angle XRD patterns of A) M2LFh, B) MSIO, and C) CIO. TEM images of b) M2LFh, c) MSIO, and d) CIO.

[*] Dr. T. Mathew,[+] K. Suzuki, Dr. Y. Ikuta, Dr. Y. Nagai, N. Takahashi, Dr. H. Shinjoh
Catalyst Laboratory, Toyota Central R&D Labs Inc.
41-1, Yokomichi, Nagakute-Cho, Aichi-ken 480-1192 (Japan)
E-mail: thomasm74@gmail.com
k-suzuki@mosk.tytlabs.co.jp

[+] Current address: Department of Nanotechnology, N. I. University Kumaracoil 629180, Tamilnadu (India)

[**] We thank Y. Itoh, N. Suzuki, Dr. T. Nonaka, and K. Fukumoto of Toyota CRDL Inc. for their valuable help in various studies.

Supporting information for this article, including details of materials synthesis and characterization and of DFT calculation, is available on the WWW under http://dx.doi.org/10.1002/anie.201102007.

of evidence that both M2LFh and MSIO are mesoporous. The low-angle XRD reflections observed for M2LFh and MSIO were supported by TEM images. The TEM images illustrate the presence of a disordered mesoporous structure in both cases (Figure 1b,c). In M2LFh, primary nanoparticles smaller than 10 nm aggregated to form a disordered mesoporous structure. In the case of MSIO, a mixture of spherical and fibrous particles was apparent. Although the above mesoporous characteristics are missing for CIO, the TEM image of CIO illustrates that it crystallized largely as tubular particles with irregular intraparticle pores (Figure 1d). The Scherrer analysis revealed that the wall structures of MSIO and CIO were made up of particles with an average crystallite size of about 8 and 18 nm, respectively. The BET surface areas of M2LFh, MSIO, and CIO were 180, 140, and 82 $m^2 g^{-1}$, respectively.

Among a wide range of materials tested at room temperature (RT), we found M2LFh to be the most efficient candidate for O_3 removal; it showed about 95% O_3 removal with high reproducibility (sample A, Figure 2). MSIO (sample B) effected an O_3 removal of 87%, whereas CIO (sample C) showed 71% removal. The O_3 elimination efficiencies of these materials were remarkably better than those of γ-Fe_2O_3 (sample D; 17.5 $m^2 g^{-1}$) and the microporous Fe-incorporated ZSM-5 (sample E, 5 wt% Fe/ZSM-5, 258 $m^2 g^{-1}$); both of these materials showed less than 5% O_3 removal at RT. Manganese oxide has been reported to be the most active oxide material for O_3 removal and is the commercial catalyst in applications such as electrostatic copying machines.[3] In our study, a commercially availed manganese oxide based O_3 removal catalyst (sample F, CMD 200, 200 $m^2 g^{-1}$, Chuo Denki Kagaku Kogyo) exhibited only about 71% removal at RT. The O_3 removal activity of other materials, such as microporous Fe–Si composites, noble-metal-supported catalysts, mesoporous and non-mesoporous oxides, and so forth, are provided in the Supporting Information (see Table S2). All of these materials showed less than 75% O_3 removal at RT.

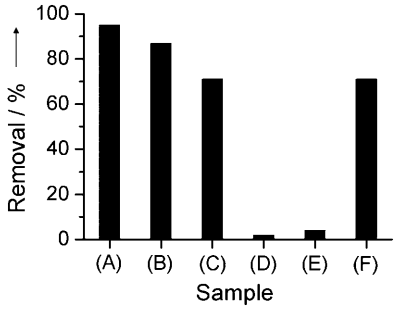

Figure 2. Comparison of the O_3 removal performances of various samples at RT: A) M2LFh, B) MSIO, C) CIO, D) γ-Fe_2O_3, E) 5 wt% Fe/ZSM-5, and F) commercial MnO_2.

We verified that the non-mesoporous 2LFh (223 $m^2 g^{-1}$) prepared by a conventional route[8] was less effective for O_3 removal than M2LFh; it showed only 71% O_3 removal at RT. This finding demonstrates that the mesoporous structure in M2LFh was advantageous in that it offered an increased number of exposed surface sites for O_3 adsorption and thereby enhanced performance in O_3 removal. The importance of mesoporous structure and the key role played by Fh nanoparticles in O_3 removal is also evident if the activity of the non-mesoporous γ-Fe_2O_3 (sample D) and MSIO are compared. The latter is mesoporous and contains about 47% Fh, although it looks like γ-Fe_2O_3 by XRD. MSIO showed about 43.5 times higher O_3 removal rate than γ-Fe_2O_3 at RT. We believe that the mesoporous structure and the characteristics of the Fh phase are useful when other gases or reactants may be included in the air stream, such as when the reaction is carried out in the presence of water vapor or if the air stream contains other contaminants as "spectator" species. For example, among all iron-based materials, M2LFh showed distinctly high activity when O_3 removal was performed at 75°C with water vapor (see Figure S3 in the Supporting Information).

We have studied the X-ray absorption characteristics of M2LFh, MSIO, and CIO to have knowledge of the relative changes in the surface and bulk structural features of these materials and accordingly of their O_3 removal performance. The Fe K-edge extended X-ray absorption fine structure (EXAFS) analysis showed softened EXAFS oscillations (Figure 3a, left) and a much lower peak intensity in the corresponding Fourier transformed (FT) spectrum at 2–4 Å (Figure 3a, right) for both M2LFh (black) and MSIO (red) in comparison with CIO (blue), thus suggesting that a long-range structural order was lacking in mesoporous Fh-based materials.[10]

A characteristic pre-edge peak in the Fe K-edge X-ray absorption near-edge structure (XANES) spectra of M2LFh, MSIO, and CIO illustrates the presence of non-centrosymmetric Fe sites in all of them (Figure 3b).[11] Of the three materials in this study, CIO with α-Fe_2O_3 phase showed the lowest pre-edge peak intensity, because the oxygen atoms in α-Fe_2O_3 are almost packed with same density around Fe^{3+} and thereby offer only a slight distortion in the octahedral (O_h) environment of Fe^{3+}.[12] Nonetheless, although M2LFh and MSIO have high surface areas and smaller particles with a lot of probable surface imperfection, we found that the pre-edge peak intensities of these materials are lower than that of pure γ-Fe_2O_3, which contains about 33% tetrahedral (T_d) iron sites. We believe that the abundant unsaturated Fe sites on the Fh particle surface have different symmetry and coordination number and thereby affect the pre-edge peak feature and its intensity differently. Unlike the case with pure γ-Fe_2O_3, where the non-centrosymmetric iron sites are more like those in the bulk, the surface-enriched Fe sites in mesostructured Fh-based materials are readily available for adsorption and reaction. Thus, M2LFh showed the highest O_3 removal activity.

Further fruitful information on the electronic states of these materials was obtained by O K-edge near edge X-ray absorption fine structure (NEXAFS) spectroscopy, which is more surface-sensitive than both EXAFS and XANES (Figure 3c). The NEXAFS spectrum of CIO showed a well-resolved splitting of Fe 3d states into t_{2g} and e_g symmetry bands in the region A (corresponding to Fe 3d + O 2p bands) with a relatively high peak intensity in the region B (corre-

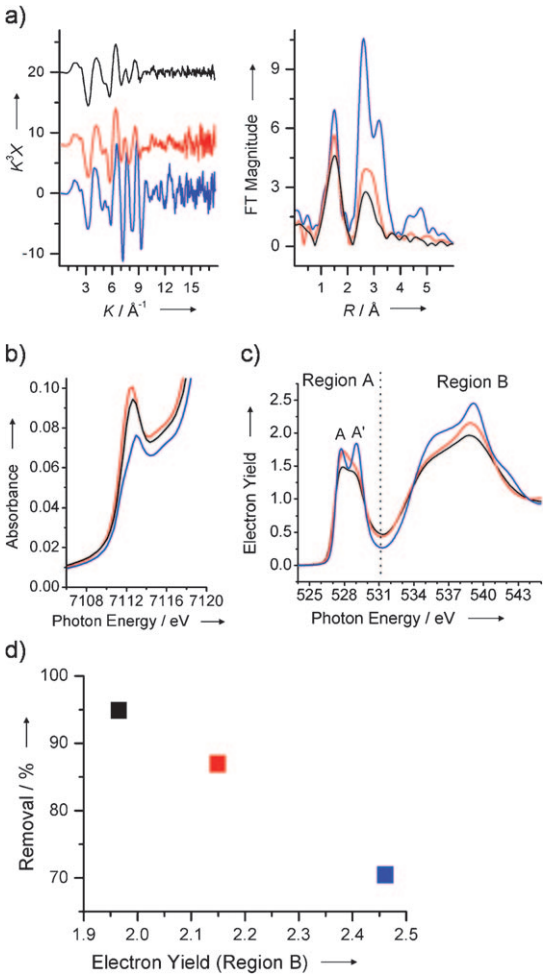

Figure 3. a) The Fe K-edge EXAFS spectra (left) and the corresponding FT spectra (right) of M2LFh (black), MSIO (red), and CIO (blue). b) The pre-edge peak from Fe K-edge XANES spectra for M2LFh (black), MSIO (red), and CIO (blue). c) The O K-edge NEXAFS spectra of M2LFh (black), MSIO (red), and CIO (blue). d) A plot of electron yield obtained from the O K-edge NEXAFS peak maximum in the region B (corresponding to Fe 4sp + O 2p states) versus O_3 removal activity for each sample at RT (indicated by the respective color). The activity decreases with relative increase of Fe 4sp contribution to the bonding.

sponding to Fe 4sp + O 2p bands).[12] This result is a clear indication of the high packing density of oxygen atoms around iron atoms in CIO. In contrast, the splitting of the 3d state is not well-resolved for M2LFh and MSIO, and a broad peak is detected with decreased intensity of the A′ peak feature. This finding is ascribed to the inherent convoluted splitting of iron in different coordination environments with less closely packed oxygen atoms and the presence of more isolated FeO_x groups[12] in M2LFh and MSIO.

Thus, the high O_3 removal activity of mesostructured Fh-based material is due to the abundantly available surface unsaturated iron sites with less oxygen packing around them and the presence of isolated FeO_x species. Probably the mesoporosity and the presence of these isolated FeO_x units in M2LFh and MSIO make them more easily reducible than CIO and other crystalline iron oxides (evidenced from temperature-programmed reduction analysis by H_2), and accordingly, they showed the highest activity (see Figure S4 in the Supporting Information). This finding is in accordance with the literature, which suggests that an easily reducible metal oxide is more active for O_3 removal and decomposition.[3] Furthermore, with respect to CIO, the relatively low peak intensity of the Fe 4sp + O 2p states in Fh-based materials (region B, Figure 3c) and the less dense packing of oxygen around iron sites indicate that the metal electrons in the latter materials are more localized around iron-atom sites. Thus, the Fe 3d + O 2p states with electrons more localized around their iron-atom sites can readily interact with electron-deficient O_3 molecules through both π and σ bonds. Contrarily, with respect to M2LFh and MSIO, the relatively high peak intensity of Fe 4sp + O 2p states of CIO suggests that there is more electron density spread to the weakly structured Fe 4sp states in the latter case. As the electron cloud in Fe 4sp + O 2p states is less localized around iron-atom sites, O_3 interaction with CIO leads to an overall smaller charge transfer from its oxide surface to the O_3 molecule. Thus, a plot of the peak maxima of the Fe 4sp + O 2p states of these iron oxides expressed in electron yield versus O_3 removal activity showed a clear trend that CIO, with the greatest contribution of Fe 4sp states, showed the lowest activity, and vice versa (Figure 3d).

On the basis of the previously proposed calculation model of Fh,[10] we have examined the interaction between O_3 and Fh(110) surface by density functional calculations (DFT) to gain a fundamental understanding of the adsorption behavior of O_3 on Fh nanoparticles. The moieties of the most stable structure that resulted after O_3 adsorption on tri- and tetracoordinated Fe sites on the Fh(110) surface are shown in Figure 4a,b. The integrated charge density difference ($\Delta\rho(\boldsymbol{r})$) for each atom of the O_3-adsorbed Fh system was calculated (see the Supporting Information for more details). A qualitative picture of the amount of electron transfer during O_3 adsorption on tri- and tetracoordinated iron sites is depicted in Figure 4c,d (the charge flows from blue to orange regions). The extent of charge (electron) transfer from O_3 to Fh ($O_3 \rightarrow$Fh) and vice versa (Fh$\rightarrow O_3$) in those adsorbed complexes were examined with Löwdin charge population (LCP) analysis, as reported in the literature.[13] This method shows that the charge population of O(I) 2p of O_3 has been increased from 4.26 to 4.59 on O_3 adsorption at tricoordinated iron sites (see Table S3 in the Supporting Information). In contrast, and with respect to gas-phase O_3, the charge densities of both the terminal oxygen atoms of O_3 at O(I) (O(III)) on tetracoordinated Fe sites has been increased to 4.56 (4.50). We observed that the magnitude of charge transfer from O_3 to Fh was smaller than that of back-donation during the adsorption process in both sites. A comparison of the bond length between gas-phase O_3 (1.28 Å) and adsorbed O_3 revealed that the O(I)–O(II) bond length (1.52 Å) of O_3 on tricoordinated sites has been elongated and that the O(II)–O(III) bond length (1.27 Å) had double-bond character, which is more or less similar to the gas-phase O_3. This result suggests that O_3 has a strong tendency to dissociate over tricoordinated iron sites, thus producing a reactive atomic "O" and an O_2 molecule (see Figure S5 in the Supporting

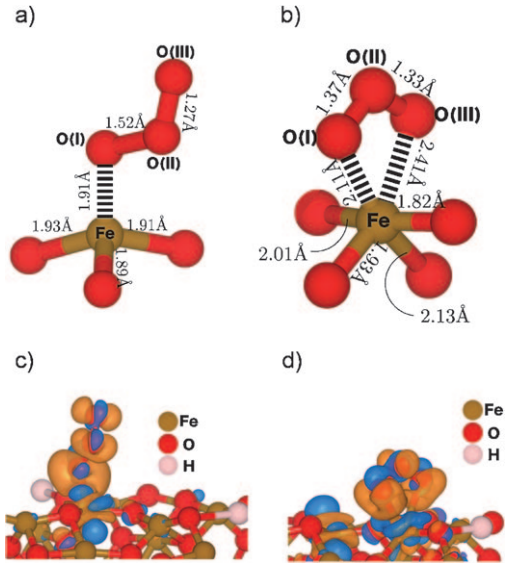

Figure 4. a) The partial structure derived from the optimized structure of O_3 adsorbed on Fh(110) tricoordinated Fe site. b) The partial structure derived from the optimized structure of O_3 adsorbed on Fh(110) tetracoordinated iron site. c, d) Charge density difference $\Delta\rho(\boldsymbol{r}) = \rho_{O_3/Fh}(\boldsymbol{r}) - \rho_{O_3}(\boldsymbol{r}) - \rho_{Fh}(\boldsymbol{r})$ for O_3 adsorbed on Fh(110), where ρ is the charge density and $\boldsymbol{r}$ denotes the position vector. The charge flows from blue regions to orange regions. c) O_3 adsorbed on Fh(110) tricoordinated iron site, and d) O_3 adsorbed on Fh(110) tetracoordinated iron site.

Information for a comparison of density of states of O_3 before and after adsorption). Although the deformation of O_3 on tetracoordinated Fe sites was less pronounced than in the case of O_3 on tricoordinated iron sites, the former case of O_3 also resulted in elongation of O–O bonds (1.33–1.37 Å) with respect to gas-phase O_3. Thus, as previously proposed,[4] the O_3 decomposition on Fh surface may proceed by an Eley–Riedel type mechanism in which the dissociatively adsorbed atomic "O" that was produced on tricoordinated iron sites or the more highly charged O_3 on tetracoordinated iron sites undergo reaction with another O_3 molecule from the gas phase, resulting in gaseous O_2 and reactive peroxide species.

In summary, we have reported for the first time the high efficiency of mesoporous two-line ferrihydrite for O_3 removal. These studies also demonstrate the promise of the highly favorable electronic and textural structures of mesoporous Fh or Fh-based iron oxides in environmental catalysis, especially for treating some of the most noxious gases in the atmosphere at moderate reaction conditions. By studying the adsorption and catalytic behavior of such a highly polarizable O_3 molecule with Fh nanoparticles, it may be possible to gain more insight into the surface structure of Fh, especially as the exact nature of the Fh surface remains ambiguous.

Experimental Section

O_3 removal measurements were carried out on a fixed-bed down-flow reactor using 0.2 g catalyst material of pellet size 0.5 mm. O_3 was generated by the electric discharge of O_2 under a suitable voltage. The resulting ($O_2 + O_3$) gas mixture at a flow rate of 0.5 L min^{-1} was then mixed with N_2 gas of flow rate 4.5 L min^{-1}, making a total gas flow rate of 5 L min^{-1} (initial concentration of O_3 was 600 ppm). The O_3 concentration was measured by a chemiluminescence method by treating the residual O_3 with 1000 ppm NO, and the O_3 removal was calculated with respect to the initial concentration.

Received: March 22, 2011
Published online: June 22, 2011

Keywords: density functional calculations · ferrihydrite · mesoporous materials · ozone · X-ray absorption spectroscopy

[1] M. Hopkin, *Nature* **2007**, *448*, 396.
[2] A. K. Sinha, K. Suzuki, *Angew. Chem.* **2005**, *117*, 275; *Angew. Chem. Int. Ed.* **2005**, *44*, 271.
[3] B. Dhandapani, S. T. Oyama, *Appl. Catal. B* **1997**, *11*, 129.
[4] W. Li, G. V. Gibbs, S. T. Oyama, *J. Am. Chem. Soc.* **1998**, *120*, 904.
[5] J. Lin, A. Kawai, T. Nakajima, *Appl. Catal. B* **2002**, *39*, 157.
[6] C. Subrahmanyam, D. A. Bulushev, L. Kiwi-Minsker, *Appl. Catal. B* **2005**, *61*, 98.
[7] H. Tüysüz, E. L. Salabasü , C. Weidenthaler, F. Schüth, *J. Am. Chem. Soc.* **2008**, *130*, 280.
[8] F. M. Michel, L. Ehm, S. M. Antao, P. L. Lee, P. J. Chupas, G. Liu, D. R. Strongin, M. A. A. Schoonen, B. L. Phillips, J. B. Parise, *Science* **2007**, *316*, 1726.
[9] M. F. Hochella Jr. , S. K. Lower, P. A. Maurice, R. L. Penn, N. Sahai, D. L. Sparks, B. S. Twining, *Science* **2008**, *319*, 1631.
[10] T. Mathew, K. Suzuki, Y. Nagai, T. Nonaka, Y. Ikuta, N. Takahashi, N. Susuki, H. Shinjoh, *Chem. Eur. J.* **2011**, *17*, 1092.
[11] L. X. Chen, T. Liu, M. C. Thurnauer, R. Csencsits, T. Rajh, *J. Phys. Chem. B* **2002**, *106*, 8539.
[12] T-J. Park, S. Sambasivan, D. A. Fischer, W.-S. Yoon, J. A. Misewich, S. S. Wong, *J. Phys. Chem. C* **2008**, *112*, 10359.
[13] D. Sanchez-Portal, E. Artacho, J. M. Soler, *Solid State Commun.* **1995**, *95*, 685.